Chapter 5

Comparing Star Formation on Large Scales in the c2d Legacy Clouds: Bolocam Surveys of Serpens, Perseus, and Ophiuchus

Abstract

We have undertaken an unprecedentedly large 1.1 millimeter continuum survey of three nearby star forming clouds using Bolocam at the Caltech Submillimeter Observatory. We mapped the largest areas in each cloud at millimeter or submillimeter wavelengths to date: 7.5 deg^2 in Perseus (chapter 2), 10.8 deg^2 in Ophiuchus (chapter 3), and 1.5 deg^2 in Serpens with a resolution of $31''$, detecting 122, 44, and 35 cores, respectively. Here we report on results of the Serpens survey and compare the three clouds. Average measured angular core sizes and their dependence on resolution suggest that many of the observed sources are consistent with power law density profiles. Tests of the effects of cloud distance reveal that linear resolution strongly affects measured source sizes and densities, but not the shape of the mass distribution. Core mass distribution slopes in Perseus and Ophiuchus ($\alpha = 2.1 \pm 0.1$ and $\alpha = 2.1 \pm 0.3$) are consistent with recent measurements of the stellar IMF, whereas the Serpens distribution is flatter ($\alpha = 1.6 \pm 0.2$). We also compare the relative mass distribution shapes to predictions from turbulent fragmentation simulations. Dense

This chapter is adapted from Enoch et al. 2007, ApJ, in press.

cores constitute less than 10% of the total cloud mass in all three clouds, consistent with other measurements of low star-formation efficiencies. Furthermore, most cores are found at high column densities; more than 75% of 1.1 mm cores are associated with $A_V \gtrsim 8$ mag in Perseus, 15 mag in Serpens, and $20 - 23$ mag in Ophiuchus.

5.1 Introduction

Large-scale physical conditions in molecular clouds influence the outcome of local star formation, including the stellar initial mass function, star-formation efficiency, and the spatial distribution of stars within clouds (e.g., Evans, 1999). The physical processes that provide support of molecular clouds and control the fragmentation of cloud material into star-forming cores has been a source of recent debate. In the classical picture magnetic fields provide support and collapse occurs via ambipolar diffusion (e.g., Shu, Adams, & Lizano, 1987), but many simulations now suggest that turbulence dominates both support and fragmentation (for a review see Mac Low & Klessen, 2004).

Dense prestellar and protostellar condensations, or cores (for definitions and an overview see Di Francesco et al., 2007), provide a crucial link between the global processes that control star formation on large scales and the properties of young stars. The mass and spatial distributions of such cores retain imprints of the fragmentation process, prior to significant influence from later protostellar stages such as mass ejection in outflows, core dissipation, and dynamical interactions. These cold (10 K), dense ($n > 10^4$ cm^{-3}) cores are most easily observed at millimeter and submillimeter wavelengths where continuum emission from cold dust becomes optically thin and traces the total mass. Thus, complete maps of molecular clouds at millimeter wavelengths are important for addressing some of the outstanding questions in star formation.

Recent advances in millimeter and submillimeter wavelength continuum detectors have enabled a number of large-scale surveys of nearby molecular clouds (e.g., Johnstone, Di Francesco, & Kirk, 2004; Kirk, Ward-Thompson, & André, 2005; Hatchell

et al., 2005; Enoch et al., 2006; Stanke et al., 2006; Young et al., 2006). In addition to tracing the current and future star-forming activity of the clouds on large scales, millimeter and submillimeter observations are essential to understanding the properties of starless cores and the envelopes of the most deeply embedded protostars (for more on the utility of millimeter observations, see Enoch et al., 2006).

We have recently completed 1.1 mm surveys of Perseus (Enoch et al., 2006, and chapter 2), Ophiuchus (Young et al., 2006, and chapter 3), and Serpens (Enoch et al., 2007, and chapter 4) with Bolocam at the Caltech Submillimeter Observatory (CSO). Unlike previous work, our surveys not only cover the largest area in each cloud to date, but the uniform instrumental properties allow a comprehensive comparison of the cloud environments in these three regions. A comparison of the results for all three clouds provides insights into global cloud conditions and highlights the influence that cloud environment has on properties of star forming cores.

The Bolocam observations of each cloud are coordinated to cover the area mapped with *Spitzer* Space Telescope IRAC and MIPS observations of Serpens, Perseus, and Ophiuchus from the "Cores to Disks" (c2d Evans et al., 2003) Legacy project. While millimeter and submillimeter observations are essential to understanding the properties of dense prestellar cores and protostellar envelopes, infrared observations are necessary to characterize the protostars embedded within those envelopes. In chapter 6 we will take advantage of the overlap between our 1.1 mm maps and the c2d *Spitzer* Legacy maps to characterize the deeply embedded and prestellar populations in the northern c2d clouds.

Our large-scale millimeter surveys of Perseus, Ophiuchus, and Serpens, completed with the same instrument and reduction techniques, provide us with a unique basis for comparing the properties of 1.1 mm emission in a variety of star-forming environments. In chapters 2–4 we presented the basic results from the three surveys. In this chapter, we examine similarities and differences in the star-forming core samples and discuss implications for physical properties of cores, global cloud conditions, and the effects of environment.

We first outline our operational definition of a millimeter core including instru-

mental effects in §5.3, and discuss the observational biases introduced by different cloud distances in §5.4. Physical implications of source sizes and shapes, and differences between the clouds, are discussed in §5.5.1. We examine source densities and compare the cloud mass versus size distributions in §5.5.2. We analyze the core mass distributions and their relation to cloud turbulence in §5.5.3, and the spatial distributions of the core samples and clustering in §5.5.4. Extinction thresholds for finding 1.1 mm cores and the efficiency of forming such cores are discussed in §5.5.5 and §5.5.6. We end with a summary in §5.6.

5.2 Three-Cloud Sample

The millimeter continuum observation of Perseus, Ophiuchus, and Serpens were described in detail in chapters 2–4. All observations were completed at $\lambda = 1.1$ mm with Bolocam[1] at the CSO. Bolocam is a large-format bolometer array that has a resolution of $31''$ at 1.1 mm and a field of view of $7\farcm5$, and was designed for mapping large fields quickly. Our surveys cover the largest areas in each cloud at millimeter or submillimeter wavelengths to date; we mapped 7.5 deg^2 in Perseus (chapter 2), 10.8 deg^2 in Ophiuchus (chapter 3), and 1.5 deg^2 in Serpens, detecting 122, 44, and 35 cores, respectively. For each cloud, the same reduction and peak-finding algorithms were applied, creating a uniform sample that is ideally suited for examining similarities and differences in the current star formation activity of these three clouds.

5.3 What is a Core?

Before comparing results from the three clouds, we first describe our operational definition of a millimeter core. The response of Bolocam to extended emission, together with observed sensitivity limits determine the type of structure that is detectable in our 1.1 mm maps. The Bolocam 1.1 mm observations presented here are sensitive to sub-structures in molecular clouds with volume density $n \gtrsim 2 \times 10^4$ cm^{-3}. One way

[1] http://www.cso.caltech.edu/bolocam

to see this is to calculate the mean density along the curve defined by the detection as a function of size in each cloud.

Figure 5.1 demonstrates how the completeness in each cloud varies as a function of source size. Plotted symbols give the total mass versus linear deconvolved size for all sources detected in each cloud, and lines indicate the empirically derived 50% completeness limits. For Ophiuchus the average completeness curve is plotted; as the rms noise varies considerably in Ophiuchus, some regions have higher or lower completeness limits than the curve shown here. Completeness is determined from Monte Carlo simulations by adding simulated sources to the raw data, processing them in the same way as the real data, and attempting to detect them using our peak-finding algorithm (see chapter 2). We are biased against detecting large diffuse sources because we detect sources based on their peak flux density, whereas the mass is calculated from the total flux, which scales approximately as the size squared.

Calculating mean densities along the 50% completeness curve in each cloud yields $n_{lim} \sim 3 - 7 \times 10^4$ cm^{-3} in Serpens, $n_{lim} \sim 2 - 4 \times 10^4$ cm^{-3} in Perseus, and $n_{lim} \sim 10 - 30 \times 10^4$ cm^{-3} in Ophiuchus. By comparison, the mean cloud density as probed by the extinction map is approximately 1000 cm^{-3} in Serpens, 220 cm^{-3} in Perseus, and 390 cm^{-3} in Ophiuchus. To be identified as a core, therefore, individual structures must have a mean density $n \gtrsim 2{\times}10^4$ cm^{-3}, and a contrast compared to the average background density of at least 30–100. The mean cloud density is estimated from the total cloud mass (§5.5.6) and assumes a cloud volume of $V = A^{1.5}$, where A is the area of the extinction map within the $A_V = 2$ contour.

Although we are primarily sensitive to cores with high density contrast compared to the background, it is clear that there is structure in the 1.1 mm map at lower contrasts as well, and that many cores are embedded within lower density filaments. The total mass in each of the 1.1 mm maps, calculated from the sum of all pixels $> 5\sigma$, is approximately twice the mass in dense cores: 176 $M_\odot$ versus 92 $M_\odot$ in Serpens, 376 $M_\odot$ versus 278 $M_\odot$ in Perseus, and 83 $M_\odot$ versus 44 $M_\odot$ in Ophiuchus, for ratios of total 1.1 mm mass to total core mass of 1.9, 1.4, and 1.9 respectively. Thus about half the mass detectable at 1.1 mm is not contained in dense cores, but is rather

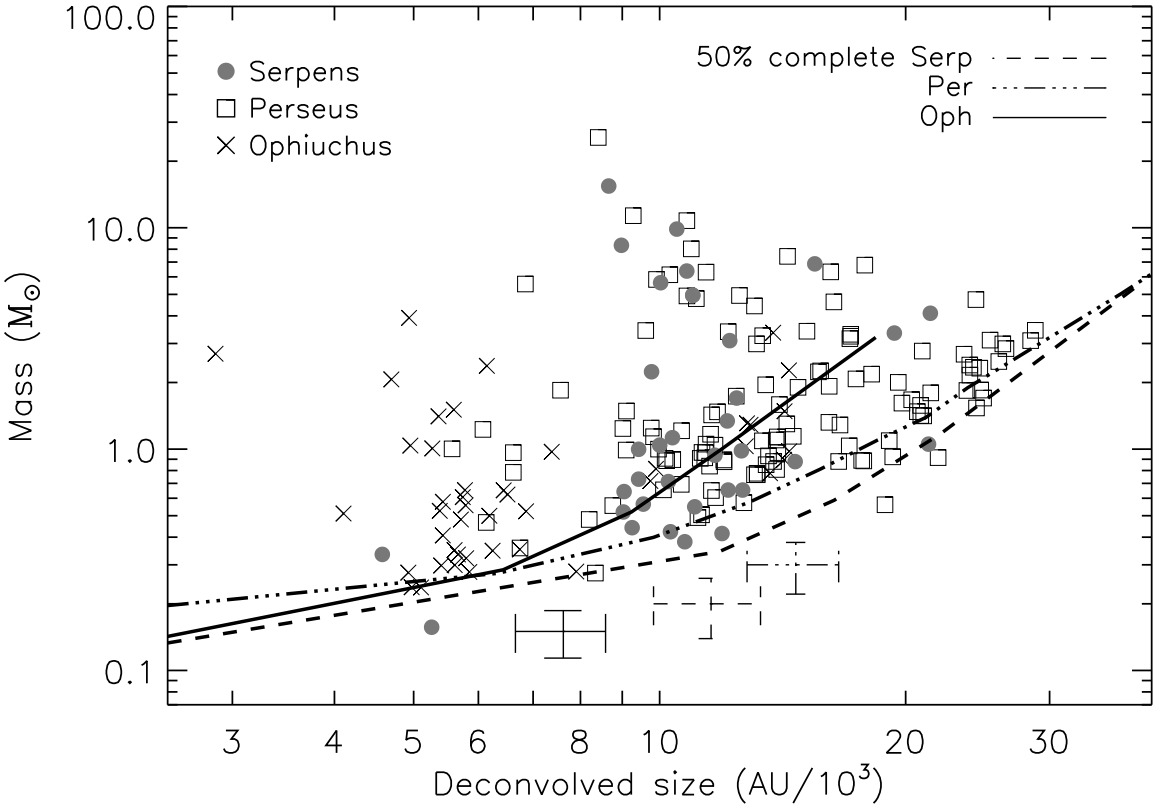

Figure 5.1 Completeness as a function of linear deconvolved source size in Serpens, Perseus, and Ophiuchus. Symbols show the distribution of source mass versus deconvolved size in each of the three clouds, where the size is the linear deconvolved average FWHM. Curves are empirical 50% completeness limits determined from Monte Carlo simulations, and demonstrate the dependence of completeness on source size and cloud distance. The beam FWHM of 31″ corresponds to approximately 8×10^3 AU in Serpens and Perseus, and 4×10^3 AU in Ophiuchus. Error bars for average sized sources near the detection limit in each cloud are also shown, as estimated from the results of Monte Carlo simulations and pointing uncertainties of approximately 10″.

in the "foothills" between high density cores and the lower density cloud medium.

Structures that meet the above sensitivity criteria and are identified by our peak-finding routine are considered cores. Our peak-finding method will cause extended filaments to be broken up into several separate "cores" if there are local maxima in the filament separated by more than one beam size, and if each has a well-defined centroid (see §4.2.4). There is some question as to whether these objects should be considered separate sources or a single extended structure, but we believe that our

method is more reliable for these data than alternative methods such as Clumpfind (Williams, de Geus, & Blitz, 1994). In chapter 2 we found that faint extended sources in our maps, which one would consider single if examining by eye, are often partitioned into multiple sources by Clumpfind. Using our method, one filamentary structure in Serpens is broken up into several sources, as are two filaments in Perseus.

Monte Carlo tests were done to quantify biases and systematic errors introduced by the cleaning and iterative mapping process, which affect the kind of structure we can detect. Measured FWHM, axis ratios, and position angles are not significantly affected by either cleaning or iterative mapping for sources with FWHM $\lesssim 120''$; likewise, any loss of flux for such sources has an amplitude less than that of the rms noise. Sources with FWHM $\gtrsim 200''$ are detected, but with reduced flux density (by up to 50%), and large errors in the measured FWHM sizes of up to a factor of two.

The limitation on measurable core sizes of approximately $120''$ corresponds to 3×10^4 AU in Perseus and Serpens, and 1.5×10^4 AU in Ophiuchus. Note that these sizes are of order the median core separation in each cloud (see §5.5.4), meaning that we are just as likely to be limited by the crowding of cores as by our sensitivity limits in the measurement of large cores. The dependence of measurable core size on cloud distance can be seen in figure 5.1, where the completeness rises steeply at smaller linear deconvolved sizes for Ophiuchus than for Perseus or Serpens. Thus we are biased against measuring large cores in Ophiuchus compared to the other two clouds. Although there are cores in our sample with sizes up to 3×10^4 AU (figure 5.1), most cores have sizes substantially smaller than the largest measurable value, again indicating that we are not limited by systematics.

To summarize, the Bolocam 1.1 mm observations presented here naturally pick out sub-structures in molecular clouds with high volume density ($n \gtrsim 2 \times 10^4$ cm^{-3}). These millimeter cores have a contrast of at least $30 - 100$ compared to the average cloud density as measured by the visual extinction map ($2 - 10 \times 10^3$ cm^{-3}). Many cores are embedded in lower density extended structures, which contribute approximately half the mass measurable in the Bolocam 1.1 mm maps. Finally, Monte Carlo tests indicate that we can detect cores with intrinsic sizes up to approximately $120''$.

5.4 Distance Effects

To test the effects of instrumental resolution and its dependence on distance, we convolve the Ophiuchus map with a larger beam to simulate putting it at approximately the same distance as Perseus and Serpens. After convolving the unfiltered Ophiuchus map to 62″ resolution, we apply the optimal filter and re-compute the local rms noise, as described for Serpens (§4.2.4). The pixel scale in the convolved map is still 10″ pixel^{-1}, but the resolution is now 62″ and the rms is lower than in the original map, with a median value of 17 mJy beam^{-1} in the main L 1688 region. Source detection and photometry is carried out in the same way as for the original map, with the exception that a 62″ beam is assumed.

We detect 26 sources in the degraded-resolution map, or 40% fewer than the 44 sources in the original map. Therefore a number of sources do become confused at lower resolution. The basic source properties for the original and degraded-resolution samples, including angular deconvolved sizes, axis ratios, mass distribution, and mean densities, are compared in figure 5.2. Here the angular deconvolved size is defined as $\theta_{dec} = \sqrt{\theta^2_{meas} - B^2}$, where θ_{meas} is the geometric mean of the measured minor and major axis FWHM sizes and B is the pointing-smeared beam FWHM (32.5″).

We note that the average source size in the degraded-resolution map is nearly twice that in the original Ophiuchus map (average angular deconvolved size of 61″ versus 98″). Such a large size difference cannot be fully accounted for by blending of sources, as even isolated sources show the same effect. This behavior provides clues to the intrinsic intensity profile of the sources. For example, a Gaussian intensity profile or a solid disk of constant intensity will both have measured deconvolved sizes that are similar in maps with 31″ and 62″ beams. Conversely, a power law intensity profile will have a larger measured size in the 62″ resolution map.

The ratio of angular deconvolved size to beam size (θ_{dec}/θ_{mb}; figure 5.3) are similar for the degraded-resolution (median $\theta_{dec}/\theta_{mb} = 1.7$) and original (median $\theta_{dec}/\theta_{mb} = 1.5$) samples, further evidence for power law intensity profiles. An intrinsic Gaussian or solid disk intensity profile will result in θ_{dec}/θ_{mb} values in the degraded-resolution

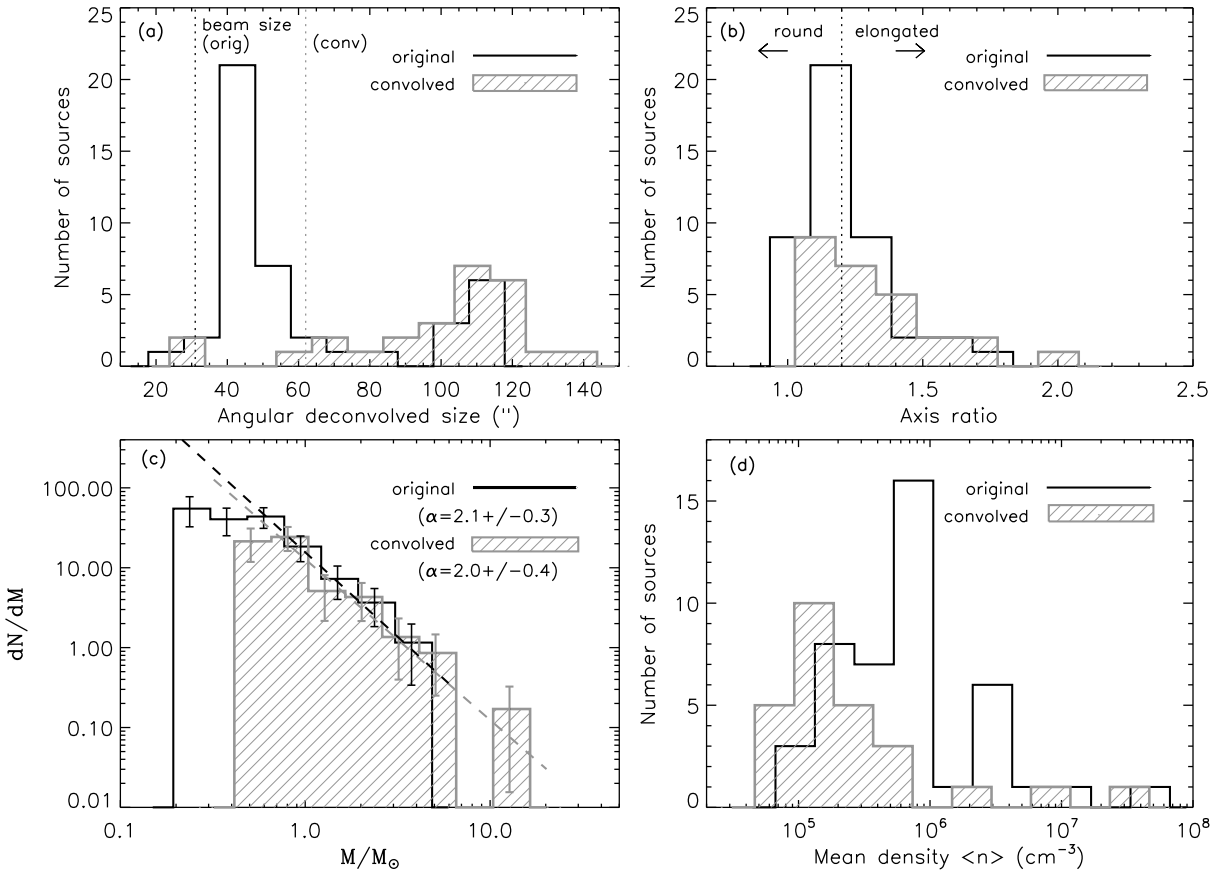

Figure 5.2 Comparison of the basic source properties for the original (black curve) and degraded-resolution, or convolved, (gray hatched curve) Ophiuchus source samples, which contain 44 and 26 cores respectively. (a) Measured angular deconvolved sizes are larger in the degraded-resolution map than in the original map by approximately a factor of two (respective mean values of 98″ and 61″). (b) Sources tend to be slightly more elongated in the degraded-resolution map, with an average axis ratio of 1.3 ± 0.2 compared to 1.2 ± 0.2 in the original map. (c) The slope of the CMD is not significantly changed for the degraded-resolution sample, but a number of low mass cores are blended into a few higher mass sources. (d) Larger deconvolved sizes lead to lower mean densities for the degraded-resolution sample (median values of 1.6×10^5 cm^{-3} and 5.8×10^5 cm^{-3}).

map that are approximately half those in the original map, while a $1/r^2$ intensity profile results in similar values in the degraded-resolution and original map (0.9 versus 1.3). We discuss source profiles further in Section 5.5.1 below.

Sources in the degraded-resolution map appear slightly more elongated, with an average axis ratio at the half-maximum contour of 1.3 ± 0.2 compared to 1.2 ± 0.2

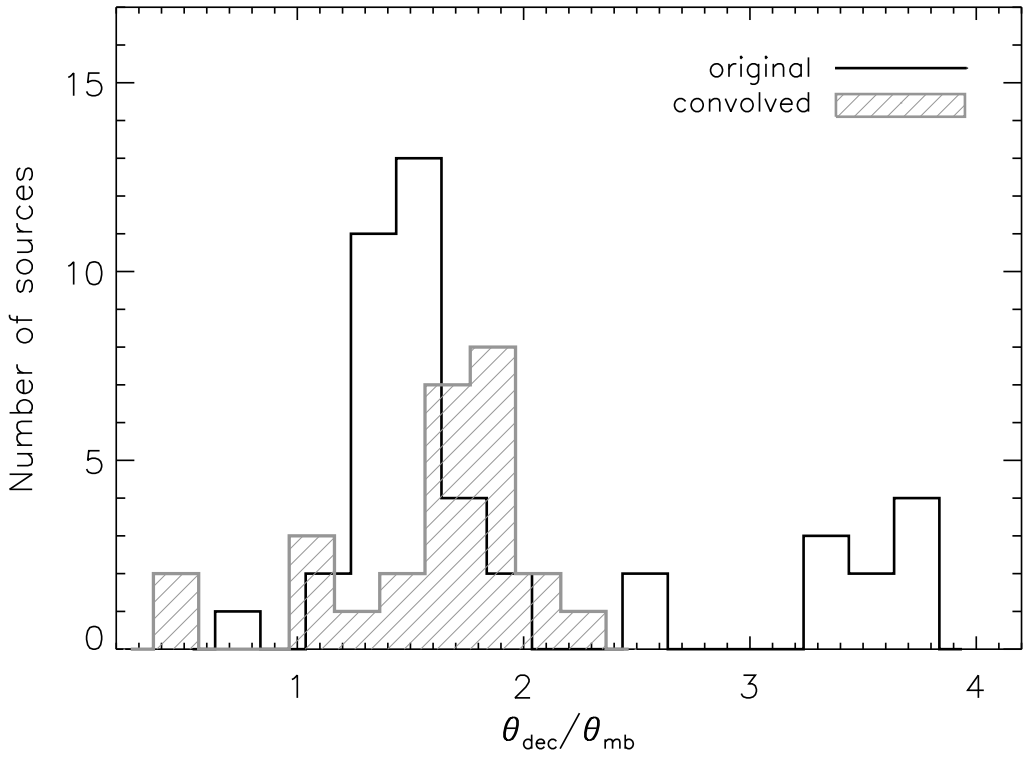

Figure 5.3 Ratio of angular deconvolved size to beam size (θ_{dec}/θ_{mb}) for the original and degraded-resolution, or convolved, Ophiuchus maps. Note that θ_{mb} is $31''$ for the original map and $62''$ for the degraded-resolution map. Measured θ_{dec}/θ_{mb} values are similar for the degraded-resolution (median $\theta_{dec}/\theta_{mb} = 1.7$) and original (median $\theta_{dec}/\theta_{mb} = 1.5$) samples, providing evidence for power law intensity profiles. An intrinsic Gaussian or solid disk intensity profile will result in θ_{dec}/θ_{mb} values in the degraded-resolution map that are nearly half those in the original map, while a $1/r^2$ intensity profile results in similar values in the degraded-resolution and original map (0.9 versus 1.3).

for the original map. Larger axis ratios are expected for blended sources in a lower-resolution map. The slope of the mass distribution is not significantly changed: 2.0 ± 0.4 for the degraded-resolution sample compared to 2.1 ± 0.3 for the original sample. The factor of two increase in deconvolved sizes do create lower mean densities in the degraded-resolution sample, however (median density of 1.6×10^5 cm^{-3} compared to 5.8×10^5 cm^{-3} for the original sample). The effect of resolution on mean densities will be discussed further in §5.5.2.

Given the small number of sources in the degraded-resolution map, we carry out

the three-cloud comparison below using the original Ophiuchus map to mitigate uncertainties from small number statistics. Any notable differences between the original and degraded-resolution Ophiuchus results will be discussed where appropriate.

5.5 Discussion

In the following sections we discuss the results of the three-cloud comparison and implications for the physical properties of cores, global cloud conditions, and the effects of environment on star formation in nearby molecular clouds.

5.5.1 Physical Implications of Source Sizes and Shapes

To compare sources in clouds at different distances, we first look at the linear deconvolved size: $D_{dec} = d\sqrt{\theta^2_{meas} - B^2}$, where d is the cloud distance, θ_{meas} is measured angular size, and B is the beam size. The distributions of linear deconvolved source sizes for the three clouds are shown in figure 5.4, left. Sources in Ophiuchus have smaller deconvolved sizes than those in Perseus or Serpens by almost a factor of two, with mean vales of 7.5×10^3 AU in Ophiuchus compared to 1.2×10^4 AU in Serpens and 1.5×10^4 AU in Perseus. There is a systematic uncertainty in the deconvolved size associated with the uncertainty in the effective beam size, which becomes larger with larger pointing errors. The effective beam in any of the three clouds may be as large as $35''$, which would decrease deconvolved sizes negligibly, by up to 10^3 AU depending on the distance and measured size.

While there are possible physical explanations for intrinsic size differences, for instance a denser medium with a shorter Jeans length should produce smaller cores on average, we are more likely seeing a consequence of the higher linear resolution in Ophiuchus, as discussed in §5.4. Thus cores in Serpens and Perseus would likely appear smaller if observed at higher resolution, and measured linear deconvolved sizes should be regarded as upper limits. To reduce the effects of distance, we examine the ratio of angular deconvolved size to beam size (θ_{dec}/θ_{mb}; figure 5.4, right). We

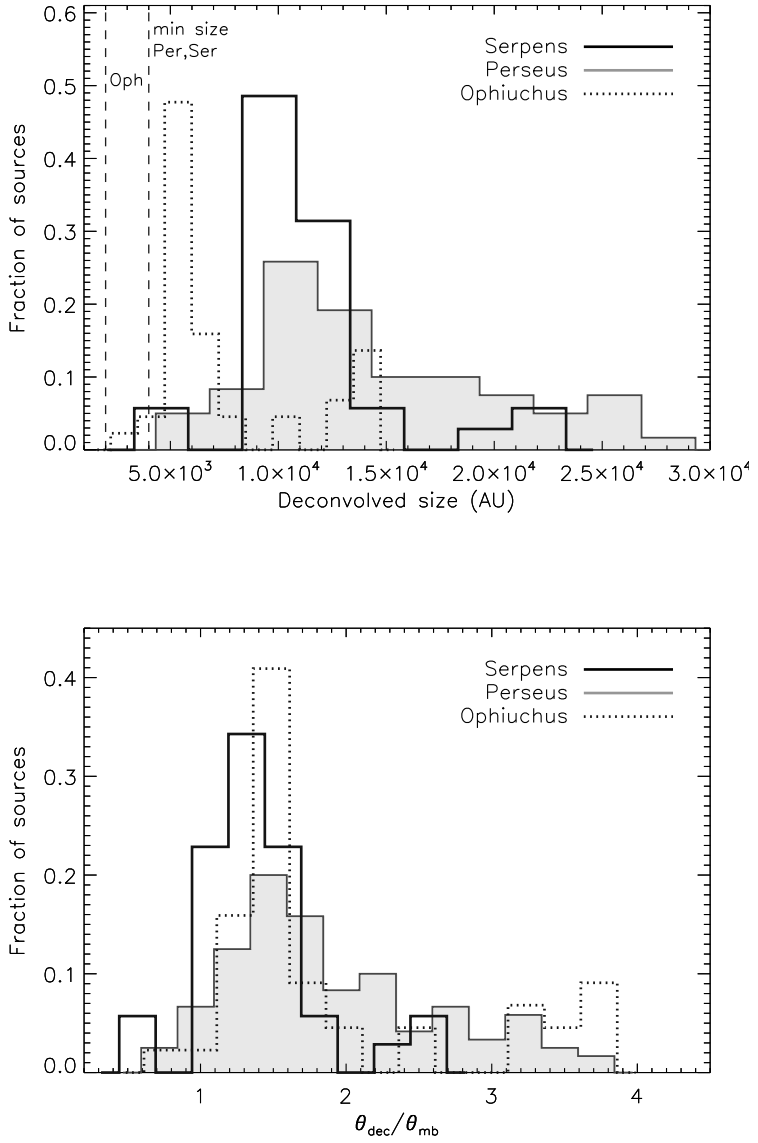

Figure 5.4 *Top*: Comparison of the distribution of deconvolved linear source sizes in Serpens (solid line), Perseus (shaded), and Ophiuchus (dotted line). Histograms are plotted as the fraction of total sources in the cloud as a function of deconvolved size in AU. Estimates of the minimum resolvable source size (dashed lines) are based on smearing of the beam by pointing errors. Although measured angular source sizes in Ophiuchus are similar to those in Perseus and Serpens, the deconvolved sizes are much smaller due to the different cloud distances. *Bottom*: Similar, but sizes are measured as the angular deconvolved size in units of the beam FWHM. For isolated sources with power law density profiles, θ_{dec}/θ_{mb} is inversely proportional to the power law index and is independent of cloud distance (Young et al., 2003).

found in §5.4 that θ_{dec}/θ_{mb} does not depend strongly on the linear resolution, but does depend on the intrinsic source intensity profile.

If the millimeter sources follow power law density distributions, which do not have a well defined size, then Young et al. (2003, hereafter Y03) show that θ_{dec}/θ_{mb} depends on the index of the power law, and not on the distance of the source. So, for example, if sources in Perseus and Ophiuchus have the same intrinsic power law profile, the mean θ_{dec}/θ_{mb} should be similar in the two clouds, and the mean linear deconvolved size should be twice as small in Ophiuchus because it lies at half the distance. This is precisely the behavior we observe, suggesting that many of the detected 1.1 mm sources have power law density profiles.

Considering that a number of the 1.1 mm sources have internal luminosity sources (see chapter 6), and that protostellar envelopes are often well described by power law profiles (Shirley, Evans, & Rawlings 2002; Y03), this is certainly a plausible scenario. According to the correlation between θ_{dec} and density power law exponent p found by Y03, median θ_{dec}/θ_{mb} values of 1.7 in Perseus, 1.5 in Ophiuchus and 1.3 in Serpens would imply average indices of $p = 1.4$, 1.5, and 1.6 respectively. These numbers are consistent with mean p values found from radiative transfer modeling of Class 0 and Class I envelopes ($p \sim 1.6$, Shirley et al. (2002); Y03), although the median for those samples is somewhat higher ($p \sim 1.8$). Note that source profiles could deviate from a power law on scales much smaller than the beam size, or on scales larger than our size sensitivity ($200''$) without affecting our conclusions.

Perseus displays the widest dispersion of angular sizes, ranging continuously from $1 - 4\theta_{mb}$. By contrast, more than half the sources in Serpens and Ophiuchus are within $0.5\theta_{mb}$ of their respective mean values. Although there is a group of Ophiuchus sources at large sizes in figure 5.4, note that the degraded-resolution Ophiuchus sample displays a very narrow range of sizes (figure 5.3), similar to Serpens. The observed size range in Perseus would correspond to a wide range of power law indices, from very shallow ($p \sim 1$) to that of a singular isothermal sphere ($p = 2$). A more likely possibility, however, is that sources with large θ_{dec}/θ_{mb} do not follow power law density profiles.

The axis ratio at the half-maximum contour is a simple measure of source shape. Figure 5.5 shows the distribution of 1.1 mm source axis ratios in the three clouds. Our simulations suggest that axis ratios of up to 1.2 can be introduced by the data reduction (chapter 2), so we consider sources with an axis ratio < 1.2 to be round, and those with a ratio > 1.2 to be elongated. Sources in Ophiuchus tend to be round, with a mean axis ratio of 1.2, but note that the mean axis ratio in the degraded-resolution Ophiuchus sample is 1.3. The average axis ratio in Serpens is 1.3, and Perseus sources exhibit the largest axis ratios with a mean of 1.4 and a tail out to 2.7.

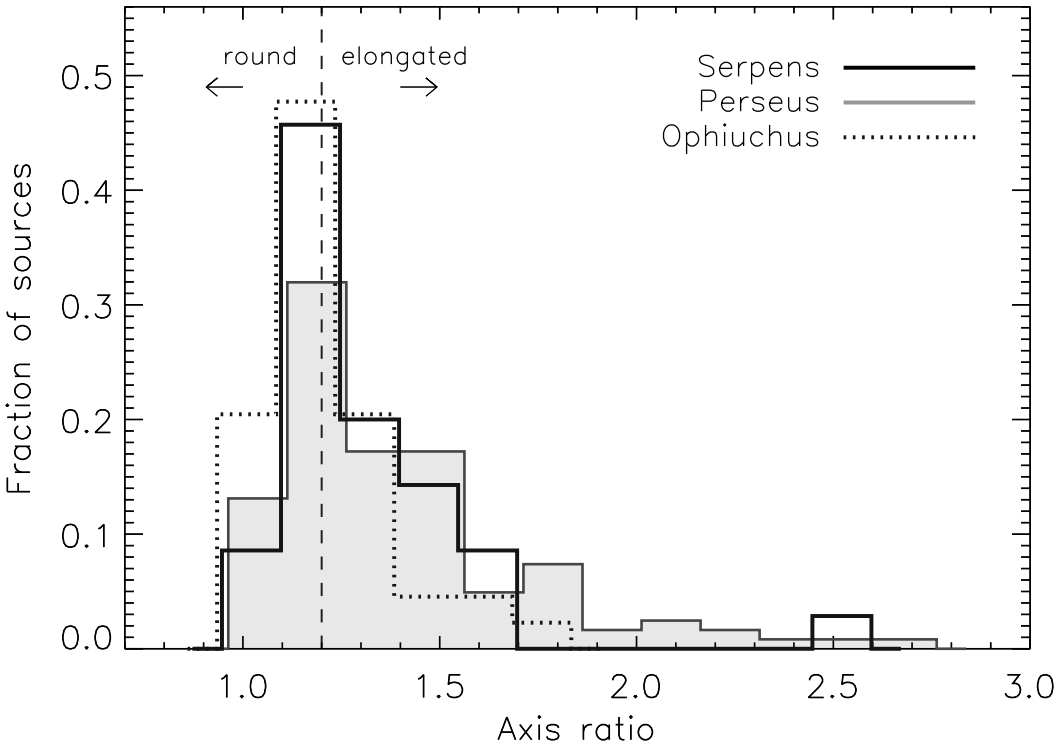

Figure 5.5 Comparison of the distribution of axis ratios, where the ratio is calculated at the half-max contour. Axis ratios < 1.2 are considered round, and $> 1/2$ elongated, based on Monte Carlo simulations. Sources are primarily round in Ophiuchus and Serpens, with mean axis ratio of 1.2 and 1.3, respectively. Perseus exhibits the most elongated sources, with a mean axis ratio of 1.4 and a distribution tail extending up to 2.7.

We found in chapter 3 that Ophiuchus sources were more elongated at the 4σ

contour than at the half-max contour, as would be the case for round cores embedded in more elongated filaments. A similar situation is seen in Serpens; the average axis ratio at the 4σ contour is 1.4 in all three clouds. Thus cores in Perseus are somewhat elongated on average, while objects in Serpens and Ophiuchus appear more round at the half-max contour but elongated at the 4σ contour, suggesting round cores embedded in filamentary structures.

In addition to angular sizes, Y03 also note a relationship between axis ratio and density power law exponent, finding that aspherical sources are best modeled with shallower density profiles. The inverse proportionality between p and axis ratio demonstrated in figure 25 of Y03 suggests power law indices in all three clouds between 1.5 and 1.7. These values are consistent with those inferred from the average angular deconvolved source sizes, and the wider variation of axis ratios in Perseus again points to a larger range in p for that cloud.

5.5.2 Densities and the Mass versus Size Distribution

Mean densities calculated using linear deconvolved FWHM sizes appear to be significantly higher in Ophiuchus, where the median of the mean densities of the sample is 5.4×10^5 cm^{-3}, than in Serpens (median density 2.2×10^5 cm^{-3}) or Perseus (median density 1.6×10^5 cm^{-3}), as seen in figure 5.6, left. There is a large scatter with standard deviation of order twice the mean value in all three clouds. Sources in Ophiuchus tend to be less massive than in the other two clouds, so the larger mean densities can be entirely attributed to smaller deconvolved sizes in the Ophiuchus sample, which are sensitive to the shape of the intrinsic density distribution (Y03). As noted in §5.4, linear resolution has a strong systematic effect on deconvolved sizes, and consequently on mean densities. The median density of the degraded-resolution Ophiuchus sample is 1.6×10^5 cm^{-3}, similar to both Perseus and Serpens.

We additionally calculate mean densities using the full-width at 4σ size rather than the FWHM size (figure 5.6, right) to test the hypothesis that mean density differences are largely an effect of how source sizes are measured. Using this definition, differences

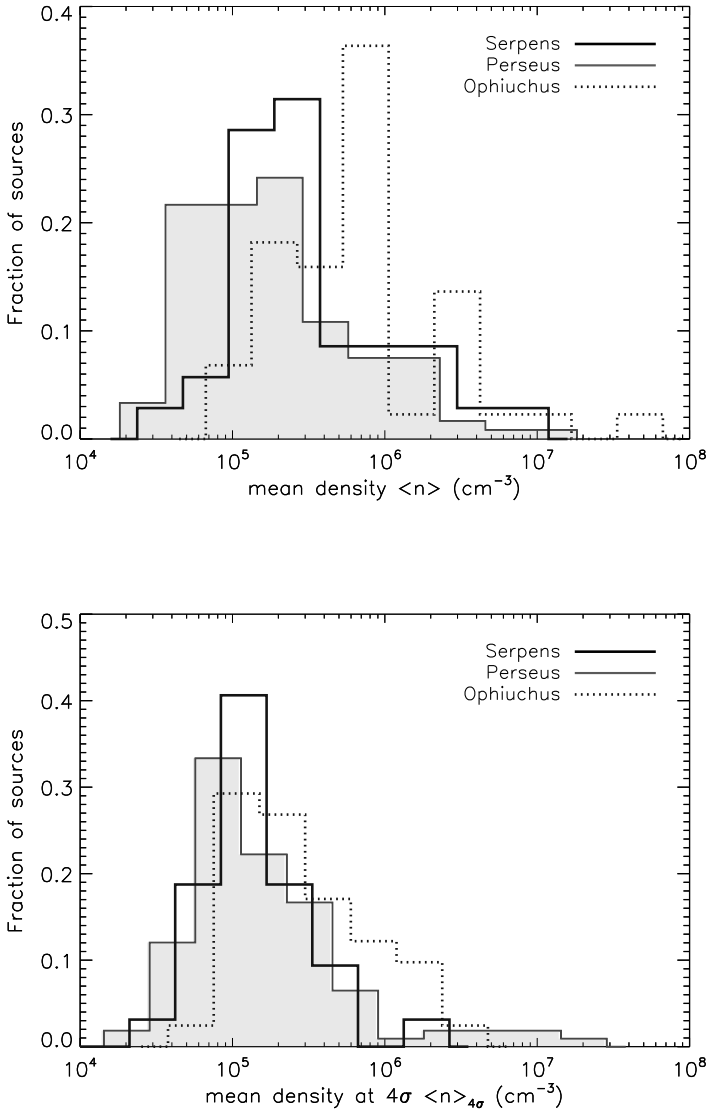

Figure 5.6 Comparison of the distributions of core mean densities. *Top:* The mean density is calculated from the total mass and the linear deconvolved source size, assuming spherical cores. Despite the lower masses of cores in Ophiuchus compared to Serpens and Perseus, mean densities in Ophiuchus are higher on average due to small linear deconvolved sizes (see figure 5.4). The mean densities in the degraded-resolution Ophiuchus sample are more consistent with Perseus and Serpens, suggesting cloud distance has a strong effect. *Bottom:* Similar, except that the mean density is calculated using the full-width at 4σ size rather than of FWHM size. Differences between the clouds are diminished; thus the mean density is less dependent on cloud distance when the source size is measured at the radius where the source merges into the background, rather than at the half-max.

between the clouds are less pronounced, with median densities of 1.2×10^5 cm^{-3} in Perseus, 1.3×10^5 cm^{-3} in Serpens, and 2.0×10^5 cm^{-3} in Ophiuchus. These numbers suggest that source mean densities are less dependent on cloud distance when measured at the radius where the source merges into the background, rather than at the half-max.

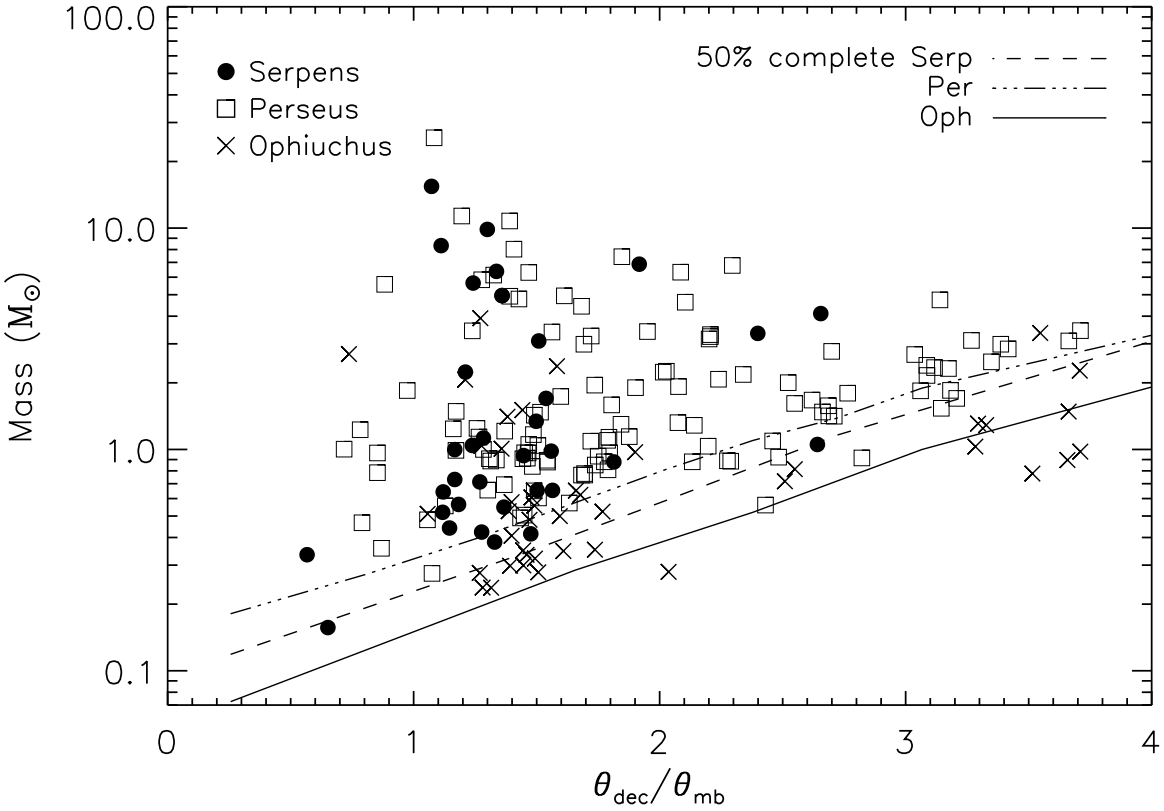

Figure 5.7 Source total mass versus angular deconvolved size (in units of the beam FWHM) for Serpens, Perseus, and Ophiuchus. The angular size is less dependent on cloud distance than the linear deconvolved source size (§5.4). Sources in Perseus fill more of the parameter space than those in Serpens or Ophiuchus, suggesting a wider range of physical conditions in that cloud. Empirically derived 50% completeness limits are also shown (lines).

Figure 5.7 again displays the source total mass versus size distribution, using the angular deconvolved size (θ_{dec}, in units of the beam size) rather than the linear deconvolved size. With the exception of two low mass compact sources, 1.1 mm sources in Serpens exhibit a wide range of masses and a narrow range of sizes. Sources in

Perseus, in contrast, demonstrate a wide range in both mass and size. This difference likely reflects a wider variety of physical conditions in the Perseus cloud, including the existence of more sources outside the main cluster regions. In such lower density regions, sources may be more extended than in densely populated groups. This idea is supported by our observations: Perseus sources within the NGC 1333 region are smaller on average (mean size of $59 \pm 13''$) than those in the rest of the cloud (mean size of $71 \pm 21''$). Sources in Ophiuchus have a more bimodal distribution, with the majority occupying a narrow range of sizes, and a smaller group with $\theta_{dec} > 3\theta_{mb}$.

5.5.3 Fragmentation and the Core Mass Distribution

Differential (dN/dM) core mass distributions (CMDs) of 1.1 mm sources in Serpens, Perseus, and Ophiuchus are shown in figure 5.8, with those of Perseus and Ophiuchus scaled down for clarity. Error bars reflect 1σ $\sqrt{N}$ statistical uncertainties. Dashed lines indicate empirical 50% completeness limits for average sized sources in each cloud, which are determined as described in §5.3 and in chapter 2. Mass distributions include all 1.1 mm cores in each cloud, including those that may be associated with embedded protostellar sources.

The shape of the Ophiuchus and Perseus mass distributions are quite similar above their respective completeness limits ($M \gtrsim 0.5$ M$_\odot$ in Ophiuchus and $M \gtrsim 0.8$ M$_\odot$ in Perseus). Fitting a power law ($dN/dM \propto M^{-\alpha}$) to the CMDs, we find that both Perseus and Ophiuchus have a best fit slope of $\alpha = 2.1$, although the error is larger on the slope for Ophiuchus ($\sigma_\alpha = 0.3$) than for Perseus ($\sigma_\alpha = 0.1$). The slope of the Serpens CMD is marginally different ($\alpha = 1.6 \pm 0.2$), being flatter than in the other two clouds by approximately 2σ.

The two-sided Kolmogorov-Smirnov test, performed on the samples of discrete masses, indicates a high probability (46%) that the Perseus and Ophiuchus mass distributions are representative of the same parent population. Conversely, the probabilities that the Serpens core masses are sampled from the same population as the Perseus (probability = 12%) or Ophiuchus (probability = 5%) masses are much lower.

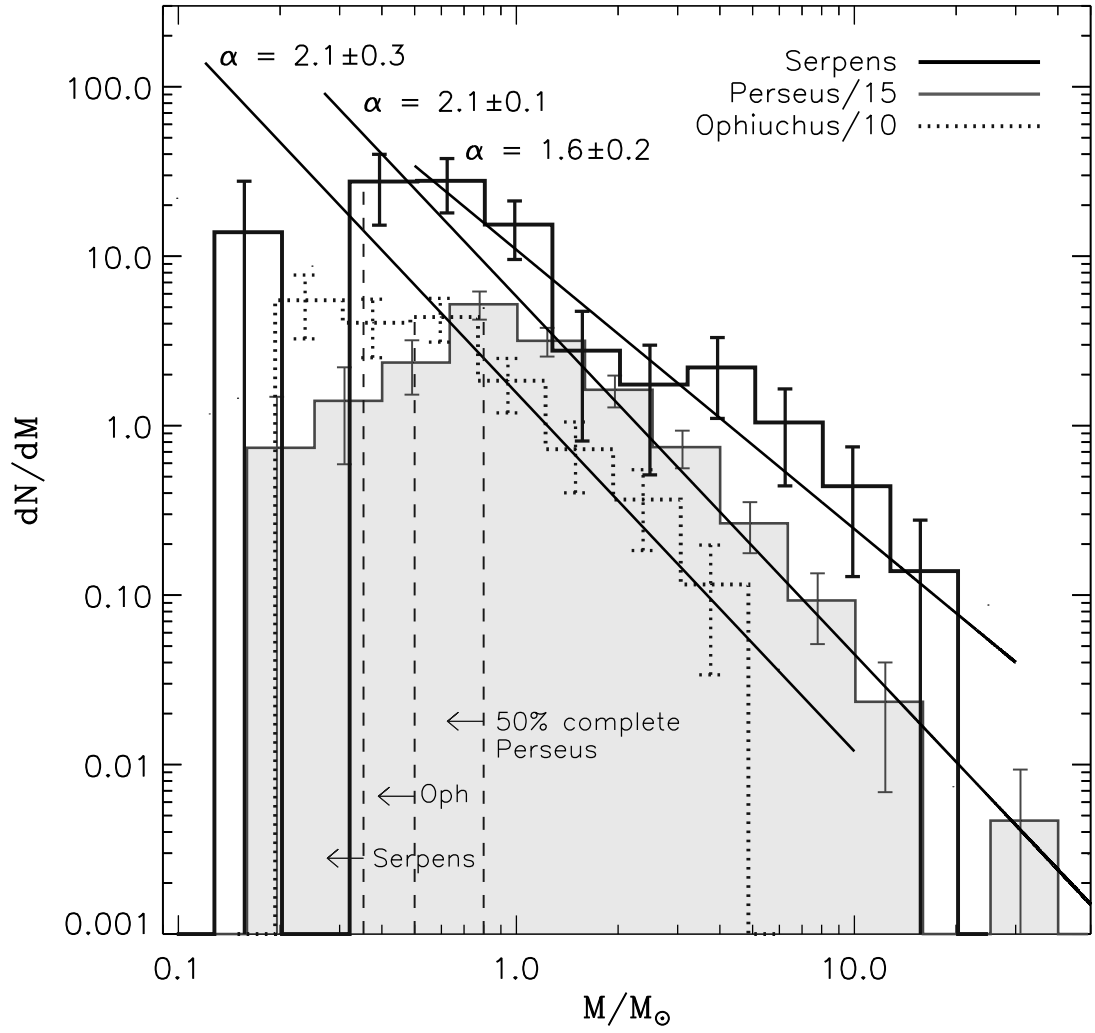

Figure 5.8 Comparison of the differential core mass distributions (CMDs) of sources in Serpens, Perseus, and Ophiuchus. The Ophiuchus curve has been scaled by 1/10, and the Perseus curve by 1/15 for clarity. Uncertainties reflect $\sqrt{N}$ counting statistics only. Vertical dotted lines show the 50% completeness limits for average sized sources in each cloud (55″ FWHM in Serpens, 68″ in Perseus and 69″ in Ophiuchus). The shape of the Perseus and Ophiuchus distributions are quite similar ($\alpha = 2.1$) in the region where both CMDs are complete. The shape of the Serpens CMD is marginally different ($\alpha = 1.6$) from the other two clouds.

Although it is possible that the lower linear resolution in Perseus and Serpens has lead to larger masses via blending, the test we conducted to increase the effective beam size in the Ophiuchus map did not appreciably change the shape of the Ophiuchus mass distribution (see figure 5.2).

If the shape of the CMD is a result of the fragmentation process, then the slope of the CMD can be compared to models, e.g., of turbulent fragmentation. Padoan & Nordlund (2002) argue that turbulent fragmentation naturally produces a power law with $\alpha = 2.3$, consistent with the slopes we measure in Perseus and Ophiuchus ($\alpha = 2.1$), but not with Serpens ($\alpha = 1.6$). Recently Ballesteros-Paredes et al. (2006, hereafter BP06) have questioned that result, finding that the shape of the CMD depends strongly on the Mach number of the turbulence in their simulations. The BP06 SPH simulations show that higher Mach numbers result in a larger number of sources with lower mass and a steep slope at the high mass end (their figure 5; see also figure 1.6). Conversely, lower Mach numbers favor sources with higher mass, resulting in a smaller number of low mass sources, more high mass cores, and a shallower slope at the high mass end.

Using an analytic argument, Padoan & Nordlund (2002) also note a relationship between core masses and Mach numbers, predicting that the mass of the largest core formed by turbulent fragmentation should be inversely proportional to the square of the Alfvénic Mach number on the largest turbulent scale $\mathcal{M}_A^2$. Given that our ability to accurately measure the maximum core mass is limited by resolution, small number statistics, and cloud distance differences, we focus here on the overall CMD shapes.

To compare our observational results to the simulations of BP06, we estimate the sonic Mach number $\mathcal{M} = \sigma_v / c_s$ in each cloud. Here σ_v is the observed rms velocity dispersion, $c_s = \sqrt{kT/\mu m_H}$ is the isothermal sound speed, and $\mu = 2.33$ is the mean molecular weight per particle. Large ^{13}CO maps of Perseus and Ophiuchus observed with FCRAO at a resolution of $44''$ are publicly available as part of "The COMPLETE Survey of Star Forming Regions"[2] (COMPLETE; Goodman, 2004; Ridge et al., 2006). Average observed rms velocity dispersions kindly provided by the COMPLETE team are $\sigma_v = 0.68$ km s^{-1} in Perseus, $\sigma_v = 0.44$ km s^{-1} in Ophiuchus, and $\sigma_v = 0.92$ km s^{-1} in Serpens (J. Pineda, personal communication). These were measured by masking out all positions in the map that have peak temperatures with a S/N less than 10, fitting a Gaussian profile to each, and taking an average of the standard deviations.

[2]http://cfa-www.harvard.edu/COMPLETE/

We note that the value of $\sigma_v = 0.68$ km s^{-1} for Perseus is smaller than a previous measurement of $\sigma_v = 2.0$ km s^{-1} based on AT&T Bell Laboratory 7 m observations of a similar area of the cloud (Padoan, Goodman, & Juvela, 2003). The smaller value derived by the COMPLETE team is most likely a consequence of the method used: a line width is calculated at every position and then an average of these values is taken. In contrast to calculating the width of the averaged spectrum this method removes the effects of velocity gradients across the cloud. The different resolutions of the surveys (44″ and 0.07 km s^{-1} for the COMPLETE observations, 100″ and 0.27 km s^{-1} for the Padoan et al. observations) may also play a role. Sources of uncertainty in the line width measurement are not insignificant, and include the possibility that ^{13}CO is optically thick to an unknown degree, and the fact that line profiles are not necessarily well fit by a Gaussian, especially in Perseus where the lines sometimes appear double peaked.

Assuming that the sound speed is similar in all three clouds, the relative velocity dispersions suggest that turbulence is more important in Serpens than in Perseus or Ophiuchus, by factors of approximately 1.5 and 2, respectively. Mach numbers calculated using the observed σ_v and assuming a gas kinetic temperature of 10 K are $\mathcal{M} = 4.9$ (Serpens), $\mathcal{M} = 3.6$ (Perseus), and $\mathcal{M} = 2.3$ (Ophiuchus). We focus on Serpens and Ophiuchus, as they are the most different. Serpens is observed to have a higher Mach number than Ophiuchus, but the CMD indicates a larger number of high mass cores, a shallower slope at the high mass end, and a dearth of low mass cores compared to Ophiuchus. This result is contrary to the trends found by BP06, which would predict a steeper slope and more low mass cores in Serpens.

One core of relatively high mass is measured in the degraded-resolution map of Ophiuchus, as is expected for blending at lower resolution (figure 5.2), making the difference between the Serpens and Ophiuchus CMDs less dramatic. The degraded-resolution CMD for Ophiuchus still has a steeper slope ($\alpha = 2.0 \pm 0.4$) than the Serpens CMD, however, and a larger fraction of low mass sources: 81% of sources in the degraded-resolution Ophiuchus sample have $M < 2M_\odot$ compared to 49% in the Serpens sample.

More accurate measurements of the Mach number and higher resolution studies of the relative CMD shapes will be necessary to fully test the BP06 prediction, given that uncertainties are currently too large to draw firm conclusions. As both numerical simulations and observations improve, however, the observed CMD and measurements of the Mach number will provide a powerful constraint on turbulent star formation simulations.

Comparing the shape of the CMD to the stellar initial mass function (IMF) may give insight into what determines final stellar masses: the initial fragmentation into cores, competitive accretion, or feedback processes. The shape of the local IMF is still uncertain (Scalo , 2005), but recent work has found evidence for a slope of $\alpha = 2.5-2.8$ for stellar masses $M \gtrsim 1$ $M_\odot$, somewhat steeper than the slopes we observe in all three clouds. For example, Reid, Gizis, & Hawley (2002) find $\alpha = 2.5$ above 0.6 $M_\odot$, and $\alpha = 2.8$ above 1 $M_\odot$. Chabrier (2003) suggests $\alpha = 2.7$ ($M > 1$ $M_\odot$), while Schröder & Pagel (2003) finds $\alpha = 2.7$ for $1.1 < M < 1.6$ $M_\odot$ and $\alpha = 3.1$ for $1.6 < M < 4$ $M_\odot$. For reference, the Salpeter IMF has a slope of $\alpha = 2.35$ (Salpeter, 1955).

For comparison to the IMF, we would ideally like to construct a CMD that includes starless cores only, so that it is a measure of the mass initially available to form a star. Although we cannot separate prestellar cores from more evolved objects with millimeter maps alone, a comparison of the Bolocam data with c2d *Spitzer* Legacy maps of the same regions will allow us to distinguish prestellar cores from those with internal luminosity sources (chapter 6).

5.5.4 Clustering

We use the two-point correlation function,

$$w(r) = \frac{H_s(r)}{H_r(r)} - 1, \tag{5.1}$$

as a quantitative measure of the clustering of cores. Here $H_s(r)$ is the number of core pairs with separation between $log(r)$ and $log(r) + dlog(r)$, and $H_r(r)$ is similar but

for a random distribution (see chapter 2). Thus $w(r)$ is a measure of excess clustering over a random distribution, as a function of separation.

Figure 5.9 plots the cloud two-point correlation functions, with the best fit power laws, $w(r) \propto r^n$, shown. The average linear source FWHM size is indicated, as well as the minimum possible separation (the beam size), and the linear map size. The best fit slopes to $w(r)$ for Serpens ($n = -1.5 \pm 0.2$), Perseus ($n = -1.18 \pm 0.06$), and Ophiuchus ($n = -1.5 \pm 0.1$) are consistent within 2σ, but there is an indication both from the slopes and a visual examination of the plot that $w(r)$ falls off more steeply in Serpens and Ophiuchus than in Perseus. A shallower slope suggests that clustering remains strong out to larger scales in Perseus than in the other two clouds.

We do find that a broken power law with slopes of $n = -0.75$ ($1.3 \times 10^4 < r < 6.3 \times 10^4$AU) and $n = -3.3$ ($r > 6.3 \times 10^4$AU) is a better fit to the Serpens correlation function than a single power law, indicating that clustering remains strong to intermediate scales, as in Perseus, but then drops off quickly. Also shown in figure 5.9 is $w(r)$ for the degraded-resolution Ophiuchus sample (gray hatched curve). The degraded-resolution sample is fit by a shallower slope ($n = -1.2 \pm 0.3$) because there are fewer sources at small separations, but it is broadly consistent with the original Ophiuchus sample.

Our general conclusion that clustering of 1.1 mm sources remains strong over larger scales in Perseus than in Serpens and Ophiuchus can also be reached by visually examining each map. Perseus has highly clustered regions spread over a larger area as well as a number of more distributed sources, whereas Serpens and Ophiuchus have a single main cluster with fewer small groups spread throughout the cloud.

A few caveats should be noted here. First, the fact that clustering seems to extend over larger scales in Perseus could simply be due to the fact that Perseus has more widely separated regions of star formation, and the physical association of all these regions has not been firmly established. Second, the map of Serpens covers a much smaller linear area than that of Perseus (30 pc^2 versus 140 pc^2); we need to be sure that the steepening of the slope in Serpens is not caused by the map size. This was confirmed by taking a piece of the Perseus map equal in size to the Serpens map and

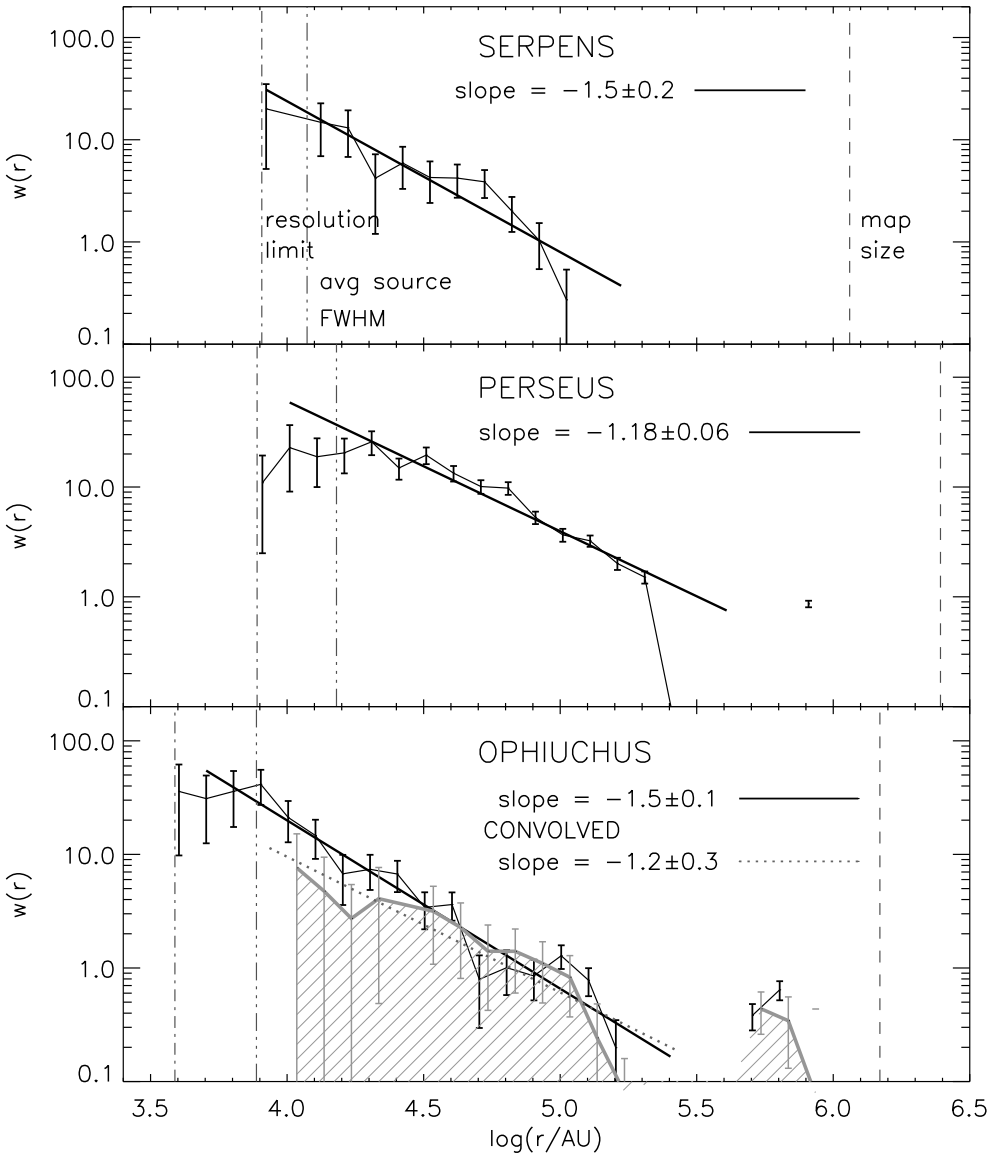

Figure 5.9 Comparison of the correlation function $w(r)$ for the three clouds, with power law fits. For each cloud the average source FWHM size, resolution limit, and linear map size in AU are indicated. The best fit slope to $w(r) \propto r^n$ is $n = -1.5 \pm 0.2$ in Serpens, $n = -1.18 \pm 0.06$ in Perseus, and $n = -1.5 \pm 0.1$ in Ophiuchus. The slope found by Johnstone et al. (2000) for a smaller map of Ophiuchus is shallower (-0.75). The slope of $w(r)$ derived for the degraded-resolution Ophiuchus sample (hatched gray curve) is also shallower (-1.2 ± 0.3), but the curve appears consistent with the original sample. Differences in the slope of the correlation function likely trace differences in clustering properties of millimeter cores in the clouds.

recalculating $w(r)$. Although the value of the slope changed slightly, the smaller map size did not cause the slope to steepen at large separations. A more serious issue is that the overall amplitude, but not the slope, of $w(r)$ depends on how large an area the random distribution $H_r(r)$ covers. We choose each random distribution such that the largest pair separation is similar to the largest pair separation in the real data. For Serpens and Ophiuchus this means that the random distribution does not cover the entire observed area.

Finally, we look at two other measures of clustering: the peak number of cores per square parsec, and the median separation of cores. Although the median separation of cores is much smaller in Ophiuchus (6.2×10^3 AU) than in Perseus (2.6×10^4 AU) or Serpens (2.3×10^4 AU), the median separation in the degraded-resolution Ophiuchus map (2.6×10^4 AU) is consistent with the other two clouds. Imposing a uniform flux limit of 75 mJy $\times$ $(\frac{250\text{pc}}{d})^2$ across all three clouds, equivalent to the 5σ limit in the shallowest map (Perseus), does not significantly change these results. The expected Jeans length in a moderately dense (mean particle density approximately 2×10^4 cm^{-3}), cool ($T \sim 10$ K) medium is $\lambda_J \sim 2.5 \times 10^4$ AU. Gravitationally-driven fragmentation can account, therefore, for the median separation of dense cores in all three clouds.

We calculate the number of cores within one square parsec at each point in the map, and take the peak value to be the peak number of cores per square parsec. The peak values are 12 pc^{-2} in Serpens, 22 pc^{-2} in Perseus, and 24 pc^{-2} in the original Ophiuchus map. Differences in linear resolution and completeness both have an effect in this case; the peak number in Ophiuchus falls to 20 pc^{-2} when using a uniform flux limit, and to 12 pc^{-2} in the degraded-resolution map. The peak number of cores per parsec provides further evidence that clustering is stronger in Perseus than in the other two clouds.

5.5.5 Relationship to Cloud Column Density

In contrast to the extinction map, which is a measure of the general cloud (line-of-sight averaged) column density, the 1.1 mm map is sensitive only to regions of high volume density (see §5.3). A comparison of the two tells us, therefore, about the relationship between dense star-forming structures and the column density of the larger-scale cloud. A visual comparison of the 1.1 mm maps of each cloud with visual extinction maps derived from the reddening of background stars (e.g., figure 4.5) suggests that 1.1 mm cores are generally found in regions of the cloud with high A_V.

Figure 5.10 quantifies the relationship between dense cores and the surrounding cloud column density by plotting the cumulative fraction of 1.1 mm cores in each cloud as a function of cloud A_V. In all three clouds the majority of cores are found at high cloud column density ($A_V > 7^m$). The A_V levels above which 75% of cores are found in each cloud are indicated by thin lines in figure 5.10: 75% of 1.1 mm cores in Perseus, Serpens, and Ophiuchus are found at visual extinctions of $A_V \gtrsim 8^m$, $A_V \gtrsim 15^m$, and $A_V \gtrsim 23^m$, respectively. Although there is not, in general, a strict extinction threshold for finding cores, below these A_V levels the likelihood of finding a 1.1 mm core is very low. Only in Ophiuchus does there appear to be a true A_V threshold; only two cores are found at $A_V < 17^m$ in this cloud.

The cumulative distribution for the degraded resolution Ophiuchus sample is nearly identical to the original Ophiuchus sample, but shifted to lower A_V by 1–2 mag. For the degraded resolution map, 75% of cores are found at $A_V \gtrsim 20^m$. Based on this result and the value for the original Ophiuchus sample, we adopt $A_V \sim 20 - 23^m$ for the 75% level in Ophiuchus. Requiring that all cores in the Perseus and Serpens sample meet the detection threshold for Ophiuchus (approximately 110 mJy) changes the distributions negligably. Only for Serpens is the 75% level increased slightly, from $A_V \sim 15^m$ to 16^m.

Cloud to cloud differences could indicate variations in the core formation process with environment, differing degrees of sub-structure in the clouds, or varying amounts of foreground extinction. Note that in chapters 2 and 3 we found extinction

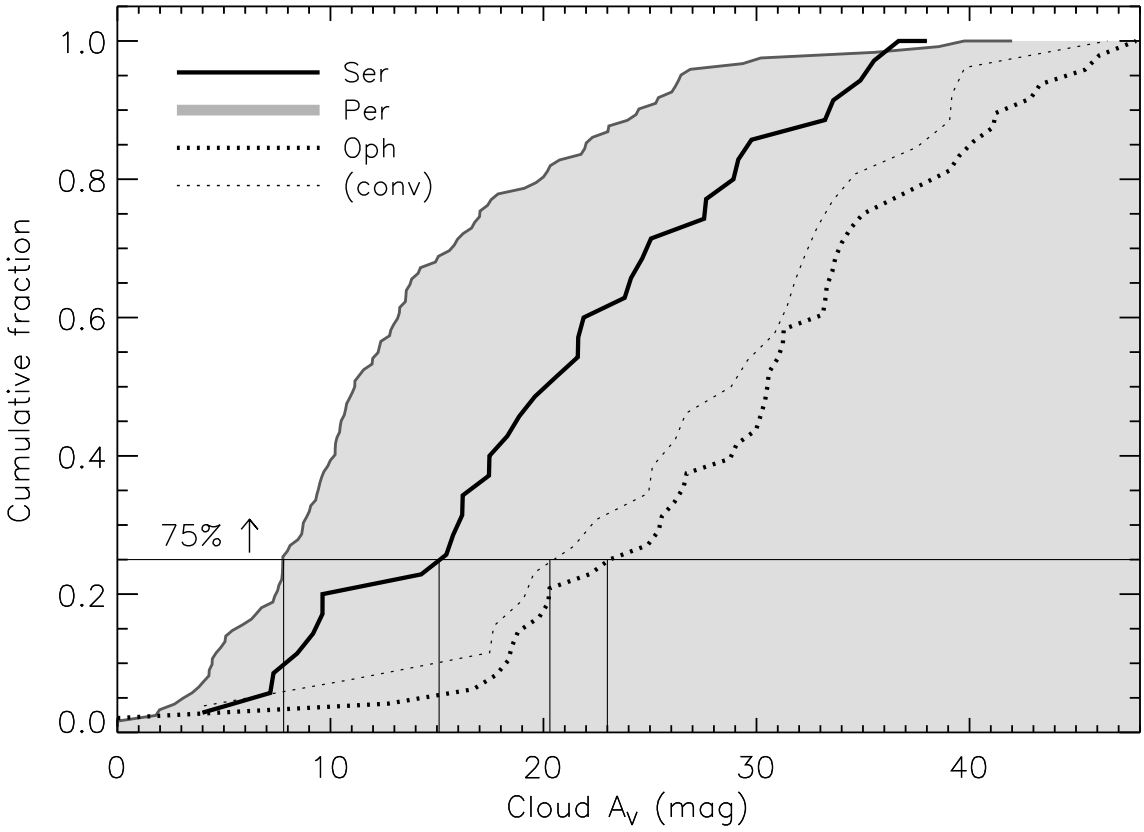

Figure 5.10 Cumulative fraction of 1.1 mm cores as a function of cloud A_V for sources in Perseus, Serpens, and Ophiuchus. The cloud A_V is derived from the reddening of background stars using 2MASS and IRAC data as described in §4.3.1. Thin solid lines denote the A_V levels above which 75% of dense cores are found in each cloud. More than 75% of 1.1 mm cores lie above $A_V \sim 8^m$ in Perseus, $A_V \sim 15^m$ in Serpens, and $A_V \sim 23^m$ in Ophiuchus. Results for the degraded resolution Ophiuchus map are shown as well (thin dotted line), but do not vary substantially from the original Ophiuchus sample, with 75% of cores above $A_V \sim 20^m$.

"thresholds" for Perseus and Ophiuchus, using a different analysis that looked at the probability of finding a 1.1 mm core as a function of A_V, of $A_V \sim 5^m$ and $A_V \sim 9^m$, respectively. Those values were derived using 2MASS-only A_V maps, rather than the c2d extinction maps used here.

Johnstone et al. (2004) have suggested an extinction threshold for forming dense cores in Ophiuchus at $A_V \sim 15^m$, based on the lowest A_V at which SCUBA cores were observed to have sizes and fluxes consistent with those of stable Bonnor-Ebert

spheres. We find that most Bolocam cores in Ophiuchus are found at even higher extinctions (75% at $A_V > 20 - 23^m$); the discrepancy likely arises from differences in the extinction maps used. Johnstone et al. (2004) used a 2MASS-derived extinction map, while the c2d extinction map used here includes IRAC data as well and probes somewhat higher A_V values. Hatchell et al. (2005) find no evidence for an extinction threshold in Perseus using 850 μm SCUBA data, but Kirk et al. (2006), also using SCUBA data, find a threshold of $A_V \sim 5^m$. Despite differences in detail, the relative 75% A_V levels found here (highest in Ophiuchus and lowest in Perseus) are consistent with the relative values of previous extinction threshold measurements in Perseus and Ophiuchus.

An extinction threshold has been predicted by McKee (1989) for photoionization-regulated star formation in magnetically supported clouds. In this model star formation is governed by ambipolar diffusion, which depends on ionization levels in the cloud. Core collapse and star formation will occur only in shielded regions of a molecular cloud where $A_V \gtrsim 4 - 8^m$. Johnstone et al. (2004) note that it is not clear how turbulent models of star formation would produce an extinction threshold for star-forming objects, and interpret such a threshold as evidence for magnetic support.

5.5.6 Efficiency of Forming Cores

Another interesting measure of global cloud conditions is the fraction of cloud mass contained in dense cores. Table 5.1 lists the cloud area and cloud mass within increasing A_V contours, calculated from the c2d visual extinction maps, as well as the total mass in cores within the same extinction contour. Cloud masses are calculated from the c2d A_V maps using $N(\mathrm{H_2})/A_V = 0.94 \times 10^{21}$ mag cm^{-2} (Bohlin, Savage, & Drake, 1978) and

$$M(\mathrm{cloud}) = d^2 m_H \mu_{H_2} \Omega \sum N(\mathrm{H_2}), \tag{5.2}$$

where d is the distance, Ω is the solid angle, $\sum$ indicates summation over all $A_V > 2$ mag pixels in the extinction map, and $\mu_{H_2} = 2.8$ is the mean molecular weight per H_2 molecule. The total cloud mass within $A_V > 2$ mag is 3470 $M_\odot$for Serpens,

Table 5.1. Cumulative mass as a function of extinction for sources in Serpens, Perseus, and Ophiuchus

Min. A_V mag	Area (%)	Cloud Mass ($M_\odot$)	Percent (%)	Core Mass ($M_\odot$)	Percent (%)	Mass Ratio[1] (%)
			Serpens			
2	100	3470	100	92	100	2.7
4	97	3420	99	92	100	2.7
6	60	2560	74	92	100	3.6
8	28	1530	44	91	98	5.9
10	15	1010	29	91	98	9.0
12	9.4	740	21	89	96	12
14	6.0	540	15	89	96	16
16	3.9	390	11	86	93	22
18	2.6	290	8.3	83	90	29
20	2.0	230	6.7	79	85	34
25	1.0	130	3.7	61	66	47
30	0.4	60	1.7	39	42	65
			Perseus			
2	100	7340	100	278	97	3.8
4	55	5460	74	273	96	5.0
6	27	3620	49	258	91	7.1
8	14	2370	32	244	86	10
10	8.0	1620	22	205	72	13
12	4.8	1140	15	161	57	14
14	3.2	840	12	127	45	15
16	2.0	610	8.3	112	39	18
18	1.3	440	6.0	96	34	22
20	0.9	340	4.6	88	31	26
25	0.4	180	2.5	53	19	29
30	0.2	100	1.4	6.1	2.2	6.1
			Ophiuchus			
2	100	3570	100	44	100	1.2
4	55	2710	76	44	100	1.6
6	25	1830	51	40	92	2.2
8	14	1330	37	40	92	3.0
10	9.0	1070	30	40	92	3.7
12	7.0	940	26	40	92	4.3
14	5.6	820	23	40	92	4.9
16	4.6	730	20	40	92	5.5
18	3.8	640	18	39	90	6.1

7340 $M_\odot$for Perseus, and 3570 $M_\odot$for Ophiuchus.

Table 5.1 (cont'd)

Min. A_V mag	Area (%)	Cloud Mass ($M_\odot$)	Percent (%)	Core Mass ($M_\odot$)	Percent (%)	Mass Ratio[1] (%)
20	3.1	560	16	37	84	6.6
25	2.0	400	11	32	73	8.0
30	1.2	260	7.3	23	52	8.8

Note. — Cloud areas and masses are calculated using the c2d extinction maps of each cloud and equation (5.2) (see §5.5.6). Core masses are taken from chapter 1 table 2.2 for Perseus, chapter 2 table 3.2 for Ophiuchus, and chapter 3 table 4.2 for Serpens.

[1]The Mass Ratio is computed from the ratio of total core mass to cloud mass within the same contour of A_V.

Within a given A_V contour, the mass ratio is defined as the ratio of total core mass to total cloud mass, and is a measure of the efficiency of core formation at that A_V level. For example, the mass ratio at the $A_V = 2$ mag contour is equivalent to the fraction of total cloud mass that is contained in dense cores. In each cloud 1.1 mm cores account for less than 5% of the total cloud mass. The mass ratios at $A_V = 2$ mag are similar in all three clouds: 3.8% in Perseus, 2.7% in Serpens, and 1.2% in Ophiuchus. If we restrict ourselves to $A_V > 6$ mag in each cloud, which is reasonable given that the Serpens map was only designed to cover $A_V > 6$ mag, the mass ratio is still low in all three clouds ($< 10\%$), and remains higher in Perseus (7%) than in Serpens (4%) or Ophiuchus (2%). Low mass ratios are consistent with measurements of the overall star-formation efficiency of $1 - 2\%$, which suggests that molecular cloud material is relatively sterile (e.g., Evans, 1999; Leisawitz, Bash, & Thaddeus, 1989).

Johnstone et al. (2004) find a mass ratio of 2.5% in a survey of approximately 4 deg^2 of Ophiuchus, quite similar to our result. Note, however, that the Johnstone et al. (2004) core masses (and mass ratio) should be multiplied by a factor of 1.5 to compare to our values, due to differences in assumed values of T_D, κ_ν, and d. In a similar analysis of 3.5 deg^2 in Perseus, also using SCUBA 850 μm data, Kirk et al. (2006) found a mass ratio for $A_V > 0$ of only 1%. The difference between this result and our value arises primarily from the smaller core masses of those authors, which

should be multiplied by 2.5 to compare to ours.

In all three clouds the mass ratio rises with increasing A_V contour, indicating that in high extinction regions a greater percentage of cloud mass has been assembled into cores, consistent with the idea that star formation is more efficient in dense regions. Although this is an intuitively obvious result, it is not a necessary one. If, for example, a constant percentage of cloud mass were contained in dense cores at all column densities, there would be a large number of dense cores lying in a low A_V background. On the other hand, a molecular cloud might consist of large regions of uniformly high extinction in which we would find no 1.1 mm cores because there is no sub-structure, and millimeter cores require high density contrast (see §5.3).

At higher A_V levels, mass ratios vary considerably from cloud to cloud. The mass ratio remains fairly low in Ophiuchus, with a maximum value of 9% at $A_V = 30$ mag. In contrast, the mass ratio rises rapidly in Serpens to 65% at $A_V = 30$ mag, which may suggest that Serpens has formed cores more efficiently than Ophiuchus at high A_V.

5.6 Summary

This work completes a three-cloud study of the millimeter continuum emission in Perseus, Ophiuchus, and Serpens. We examine similarities and differences in the current star formation activity within the clouds using large-scale 1.1 mm continuum maps completed with Bolocam at the CSO. In total, our surveys cover nearly 20 deg^2 with a resolution of 31″ (7.5 deg^2 in Perseus, 10.8 deg^2 in Ophiuchus, and 1.5 deg^2 in Serpens), and we have assembled a sample of 200 cores (122 in Perseus, 44 in Ophiuchus, and 35 in Serpens). Point mass detection limits vary from approximately 0.1 to 0.2 $M_\odot$ depending on the cloud. The results presented here provide an unprecedented global picture of star formation in three clouds spanning a range of diverse environments.

These Bolocam 1.1 mm observations naturally select dense cores with $n \gtrsim 2 \times 10^4$ cm^{-3} and density contrast compared to the background cloud of at least 30 −

100. We test instrumental biases and the effects of cloud distance by degrading the resolution of the Ophiuchus map to match the distance of Perseus and Serpens. We find that linear resolution strongly biases measured linear deconvolved source sizes and mean densities, but not the mass distribution slope. Angular deconvolved sizes are less strongly affected by cloud distance.

Rather than a true physical difference, the small mean linear deconvolved sizes in Ophiuchus (0.8×10^4 AU) compared to Perseus (1.5×10^4 AU) and Serpens (1.2×10^4 AU) are likely a result of observing sources with power law density profiles, which do not have a well defined size, at a distance of 125 pc in Ophiuchus versus 250 pc in Perseus and 260 pc in Serpens. The observed mean angular deconvolved sizes and axis ratios in each cloud suggest average power law indices ranging from $p = 1.4$ to 1.7 (Y03).

Sources in Perseus exhibit the largest range in sizes, axis ratios, and densities, whereas sources in both Serpens and Ophiuchus display a fairly narrow range of sizes for a large range of masses. We suggest that this is indicative of a greater variety of physical conditions in Perseus, supported by the fact that Perseus contains both dense clusters of millimeter sources and more isolated distributed objects. A wide range in angular deconvolved sizes may also imply a range in the power law index of source profiles in Perseus (Y03).

The slope of the clump mass distribution for both Perseus and Ophiuchus is $\alpha = 2.1$, marginally different than the Serpens slope of $\alpha = 1.6$. Only Perseus and Ophiuchus are consistent within the substantial errors with the stellar initial mass function ($\alpha \sim 2.5 - 2.8$) and with the slope predicted for turbulent fragmentation ($\alpha = 2.3$) by Padoan & Nordlund (2002).

Turbulent fragmentation simulations by BP06 predict that higher cloud Mach numbers should result in a large number of low mass cores, and low Mach numbers in a smaller number of higher mass cores. Given the measured Mach numbers of $\mathcal{M} = 4.9$ in Serpens, 3.6 in Perseus and 2.3 in Ophiuchus, our observed core mass distribution (CMD) shapes are inconsistent with the turbulent fragmentation prediction from BP06. We cannot rule out a turbulent fragmentation scenario, however,

due to uncertainties in the observations and in our assumptions.

We argue that clustering of 1.1 mm sources remains stronger out to larger scales in Perseus, based on the slope of the two-point correlation function (-1.5 in Serpens and Ophiuchus, and -1.2 in Perseus). This result is supported by the fact that the peak number of cores per square parsec is larger in Perseus (22 pc^{-2}) than in Serpens (12 pc^{-2}) or the degraded-resolution Ophiuchus map (12 pc^{-2}).

Finally, we examine relationship between dense cores and the local cloud column density, as measured by visual extinction (A_V). Extinction thresholds for star formation have been suggested based on both theory and observation (McKee, 1989; Johnstone et al., 2004). Although in general we do not observe a strict A_V threshold, dense 1.1 mm cores do tend to be found at high A_V: 75% of cores in Perseus are found at $A_V \gtrsim 8^m$, in Serpens at $A_V \gtrsim 15^m$, and in Ophiuchus at $A_V \gtrsim 20 - 23^m$. Our results confirm that forming dense cores in molecular clouds is a very inefficient process, with 1.1 mm cores accounting for less than 10% of the total cloud mass in each cloud. This result is consistent with measurements of low star formation efficiencies of a few percent from studies of the stellar content of molecular clouds (e.g., Evans, 1999).

While millimeter-wavelength observations can provide a wealth of information about the detailed properties of star forming cores as well as insight into the large scale physical properties of molecular clouds, they do not tell a complete story. Detecting and understanding the youngest embedded protostars currently forming within those cores requires information at mid- to far-infrared wavelengths. The Bolocam maps for all three clouds presented here are coordinated to cover the same regions as the c2d *Spitzer* Legacy IRAC and MIPS maps of Serpens, Perseus, and Ophiuchus. Combining millimeter and *Spitzer* data for these clouds will allow us to separate starless cores from cores with embedded luminosity sources and to better understand the evolution of cores through the early Class 0 and Class I protostellar phases (chapter 6).

Acknowledgments

The authors are grateful to Paul Harvey, Yancy Shirley, and an anonymous referee for comments that significantly improved this work. We thank members of the Bolocam team for instrumental and software support. We also thank the Lorentz Center in Leiden for hosting several meetings that contributed to this paper. Support for this work, part of the Spitzer Legacy Science Program, was provided by NASA through contracts 1224608 and 1230782 issued by the Jet Propulsion Laboratory, California Institute of Technology, under NASA contract 1407. Bolocam was built and commissioned under grants NSF/AST-9618798 and NSF/AST-0098737. KEY was supported by NASA under Grant NGT5-50401, issued through the Office of Space Science. Additional support came from NASA Origins grant NNG04GG24G to NJE and NSF grant AST 02-06158 to JG. MLE acknowledges support of a Moore Fellowship and an NSF Graduate Research Fellowship.

Bibliography

Ballesteros-Paredes, J., Gazol, A., Kim, J., Klessen, R. S., Jappsen, A-K., & Tejero, E., 2006, ApJ, 637, 384

Bohlin, R. C., Savage, B. D., & Drake, J. F. 1978, ApJ, 224, 132

Chabrier, G. 2003, PASP, 115, 763

Di Francesco, J., Evans, N. J., II, Caselli, P., Myers, P. C., Shirley, Y., Aikawa, Y., & Tafalla, M. 2007, in Protostars and Planets V, editors B. Reipurth, D. Jewitt, and K. Keil, p. 17

Enoch, M. L., Young, K. E., Glenn, J., Evans, N. J., II, Golwala, S., Sargent, A. I., Harvey, P., et al. 2006, ApJ, 638, 293

Enoch, M. L., Glenn, J., Evans, N. J., II, Sargent, A. I., Young, K. E., & Huard, T. L. 2007, ApJ, in press

Evans, N. J., II 1999, ARA&A, 37, 311

Evans, N. J., II, Allen, L. E., Blake, G. A., Boogert, A. C. A., Bourke, T., Harvey, P. M., Kessler, J. E., et al. 2003, PASP, 115, 965

Goodman, A. A., 2004, in Star Formation in the Interstellar Medium, ASPC, 323, 171

Hatchell, J., Richer, J. S., Fuller, G. A., Qualtrough, C. J., Ladd, E. F., & Chandler, C. J. 2005, A&A, 440, 151

Johnstone, D., Di Francesco, J., & Kirk, H. 2004, ApJ, 45, 611L

Johnstone, D., Wilson, C. D., Moriarty-Schieven, G., Joncas, G., Smith, G., Gregersen, E., & Fich, M. 2000, ApJ, 545, 327

Kirk, J. M., Ward-Thompson, D., & André, P. 2005, MNRAS, 360, 1506

Kirk, H., Johnstone, D., & Di Francesco, J. 2006, ApJ, 646, 1009

Leisawitz, D., Bash, F., & Thaddeus, P. 1989, ApJS, 70, 731

Mac Low, M.-M. & Klessen, R. S. 2004, Reviews of Modern Physics, 76, 125

McKee, C. F. 1989, ApJ, 345, 782

Padoan, P., Goodman, A. A., & Juvela, M. 2003, ApJ, 588 881

Padoan, P., & Nordlund, Å. 2002, ApJ, 576, 870

Reid, I. N., Gizis, J. E., & Hawley, S. L. 2002, AJ, 124, 2721

Ridge, N. A., et al. 2006, AJ, 131, 2921

Salpeter, E. E. 1955, ApJ, 121, 161

Scalo, J., 2005 in The Stellar Initial Mass Function Fifty Years Later, Kluwer Academic Publishers, editors E. Corbelli, F. Palla, and H. Zinnecker, p. 23

Schröder, K.-P.,& Pagel, B. E. J. 2003, MNRAS, 343, 1231

Shirley, Y. L., Evans, N. J., II, & Rawlings, J. M. C. 2002, ApJ, 575, 337

Shu, F. H., Adams, F. C., & Lizano, S. 1987, ARA&A, 25, 23

Stanke, T., Smith, M. D., Gredel, R., Khanzadyan, T. 2006, A&A, 447, 609

Williams, J. P., de Geus, E. J., & Blitz, L. 1994, ApJ, 428, 693

Young, C. H., Shirley, Y. L., Evans, N. J., II, & Rawlings, J. M. C. 2003, ApJS, 145, 111

Young, K. E., Enoch, M. L., Evans, N. J., II, Glenn, J., Sargent, A., Huard, T. L., Aguirre, J., et al. 2006, ApJ, 644, 326